symmetry

MDPI

Article

Fault-Tolerant Phototaxis of a Modular System Inspired by *Gonium pectorale* Using Phase-Based Control

Kohei Nishikawa *, Yuki Origane, Hiroki Etchu and Daisuke Kurabayashi

Department of Systems and Control Engineering, School of Engineering, Tokyo Institute of Technology, Meguro-ku, Tokyo 152-8550, Japan; origane@irs.sc.e.titech.ac.jp (Y.O.); etchu@irs.sc.e.titech.ac.jp (H.E.); dkura@irs.sc.e.titech.ac.jp (D.K.)

* Correspondence: nishikawa.k@irs.sc.e.titech.ac.jp

Abstract: In this study, we proposed a model for modular robots in which autonomous decentralized modules adaptively organize their behavior. The phototaxis of *Gonium pectorale*, a species of volvocine algae, was modeled as a modular system, and a fault-tolerant modular control method of phototaxis was proposed for it. The proposed method was based on the rotation phase of the colony and adaptively adjusted an internal response-related parameter to enhance the fault tolerance of the system. Compared to a constant parameter approach, the simulation results demonstrated a significant improvement in the phototaxis time for positive and negative phototaxis during module failures. This method contributes to achieving autonomous, decentralized, and purposeful mediation of the modules necessary for controlling modular robots.

Keywords: modular robotic system; phototaxis; phase modeling

Citation: Nishikawa, K.; Origane, Y.; Etchu, H.; Kurabayashi, D. Fault-Tolerant Phototaxis of a Modular System Inspired by *Gonium pectorale* Using Phase-Based Control. *Symmetry* **2024**, *16*, 630. https://doi.org/10.3390/sym16050630

Academic Editors: Jin Tao and Yumin Zheng

Received: 12 April 2024
Revised: 1 May 2024
Accepted: 6 May 2024
Published: 19 May 2024

1. Introduction

Robots operating in harsh environments, such as disaster sites, underwater, or outer space, require high adaptability, robustness, and fault tolerance. They must function with little to no maintenance for long periods, even if some malfunctions occur.

Modular reconfigurable robots (MRRs) [1,2] and modular self-reconfigurable robots (MSRs) [3,4] have been developed for this purpose. M-TRAN [5–7] achieved high environmental adaptability in terms of mobility by changing the manner the modules were assembled according to the surrounding environment. Recently, FireAntV3 enabled module-to-module coupling without requiring alignment, irrespective of its orientation or location [8]. These MRRs and MSRs focused on the mechanism of combining modules and degrees of freedom to realize their functions. On the other hand, in these studies, the behavior of each module after reconfiguration is often predetermined.

In recent modular robot research, various control strategies for modules after configuration have also been proposed. Various researchers have worked on the development of evolutionary algorithms to generate control methods for modular robots [9]. Other works have proposed optimization methods for control parameters for each module of modular robot manipulators [10] and the generation of control policies and configuration design using reinforcement learning algorithms [11,12]. In the field of underwater modular robots that we address in this study, Doyle et al. have proposed modular fluidic propulsion (MFP) [13]. This research proposed autonomous distributed control rules for modules. Some works interpreted module configurations as graph structures for kinematics analysis or machine learning [11,14].

Most of the control policies proposed by these studies assumed fault-free conditions. To explore extreme environments, a modular robot must achieve fault-tolerant, autonomous, and decentralized control among its modules. In the field of swarm robotics, kilobots [15,16] have developed a self-organizing system that complements a failing agent. Particle robotics [17] is an approach for robot control involving failed modules, which is

based on statistical mechanisms and aims to control groups of smaller, simpler, and more numerous robots.

The value of modular robots can be further enhanced if modules can autonomously function and form groups of robots that exhibit purposive behavioral order for the entire colony. In this study, we model and control methods for underwater modular robots that are autonomous, decentralized, and robustly purposive by self-organizing the behavioral order of the entire colony.

As a model organism, we focused on Gonium owing to its suitable properties. Gonium is a species of Volvocine algae, as shown in Figure 1a. Volvocine algae, which are phototactic with numerous somatic cells, range from unicellular organisms, such as Chlamydomonas [18], to multicellular ones, such as Volvox [19], which comprise 1000 to 5000 somatic cells. Most Volvocine algal species exhibit phototaxis. Gonium consists of 8–16 almost identical cells and exhibits phototaxis without intercellular communication. Asymmetric Gonium (Figure 1b) exhibits phototaxis even with immobile cells or cells that have dropped out of the colony [20]. Therefore, Gonium phototaxis is a fault-tolerant, autonomous, and decentralized control system suitable as a model for modular robots.

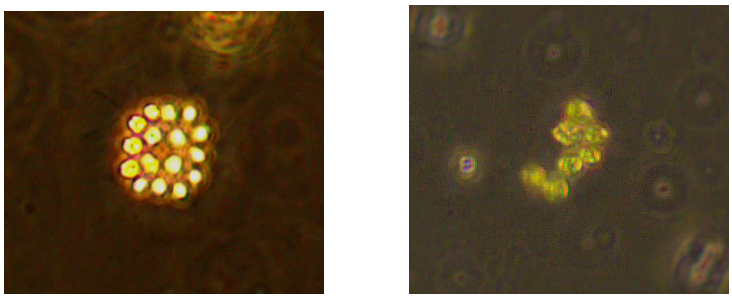

(**a**) (**b**)

Figure 1. View of Gonium (*Gonium pectorale*). (**a**) Complete organism comprising 16 cells. (**b**) Asymmetrical organism where several cells have dropped out.

We aimed to achieve fault-tolerant modular robots by adaptively controlling each module according to the overall state of the entire colony. In this study, we considered the phototaxis of Volvocine algae and modeled its body structure and swimming behavior using phase representation. We then proposed a control model and parameter-tuning method to maintain a robust phototaxis response to the failure of some modules. Simulations were performed to confirm the validity of the model. Our study is a novel contribution to robotics, which establishes autonomous, decentralized, and fault-tolerant control.

2. Problem Settlement

2.1. Phototaxis of Gonium pectorale

Gonium is a fault-tolerant autonomous decentralized control system, which is a suitable model for modular robots. Figure 2 shows the body structure of Gonium. Individual cells of Gonium have one eye spot as a light sensor and two flagella for propulsion and rotation [21]. Gonium colonies consist of cells in a disk form, as shown in Figure 2. As Gonium is structured like a cluster of unicellular organisms that are nearly identical to Chlamydomonas, its dynamics can be modeled as that of a modular system.

Gonium swims perpendicular to the disk, rotating clockwise (when viewed from the direction of swimming). Somatic cells of Gonium exhibit distinct flagellar motion [22]. The four central cells perform an opposing breaststroke, aiding propulsion but not affecting rotation or phototaxis. Conversely, the flagella of the 12 peripheral cells operate in parallel, facilitating phototaxis, rotation, and propulsion [23]. Micropipette experiments have revealed that as the eye spot of an individual peripheral cell receives light stimulation, the cell slows down its flagellar beating frequency [20]. As the propulsion force of the flagella directly depends on its beating frequency, the propulsion of the light-side cells decreases,

and the entire colony reorients its swimming direction toward the light. This mechanism allows autonomous and decentralized phototaxis without cell-to-cell communication.

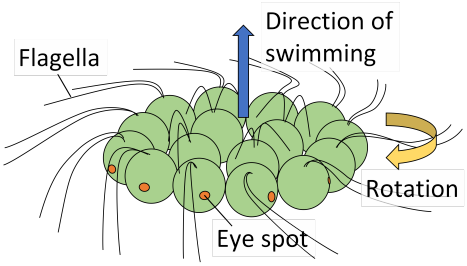

Figure 2. Schematic of a colony. One cell has two flagella for propulsion and an eye spot. The colony rotates and swims in the directions indicated by the yellow and blue arrows, respectively.

It is important to note that Gonium exhibits phototaxis even when propulsive forces are unbalanced owing to immobile or dropped cells. In contrast, a previous study [20] modeling the dynamics of Gonium suggested that an imbalance among cells improves phototaxis performance. Thus, Gonium is a suitable model for modular robots.

Mathematical models have been proposed to reproduce the trajectories of the phototactic Gonium [20]. However, these did not model the phototaxis of Gonium as a response of individual cells but as the response of a continuous colony. We constructed our model based on this reference [20] but as a colony of autonomous individual modules (cells).

The eyespot of Chlamydomonas is located 45° from the cis-flagellum [18]. A study on Gonium by Maleprade et al. [20] considered the rotation of the eye spot.

Studies have investigated the effects of rotational angular velocity and response delay time on the phototaxis of Volvocine algae. A study on Chlamydomonas [24] highlighted the impact of the response delay time for light on phototaxis and suggested that the efficiency of phototactic behavior changed with delay time, enabling switches between positive and negative phototaxis depending on the conditions. Furthermore, changes in the rotation period affected the phototaxis of Volvocine algae [25]. The timescale of the photoresponse of Volvocine algae can be tuned according to the rotation period [26]. This evidence underscores the significance of addressing the delay time and rotation rate.

2.2. Model Design Specification and Constrains

To accurately model the phototaxis swimming dynamics of Gonium as a modular system, we designed a modular system that adheres to specific constraints:

- A Gonium colony comprises multiple identical modules.
- Every module operates autonomously, with its own inputs and outputs.
- Modules function independently without communication between them.
- The model's physical structure closely mimics that of real Gonium.

To ensure our model's fidelity to real Gonium, we set the following design specifications, informed by [20,27]:

- Colonies consist of 16 spherical modules arranged in a rigid disk shape, with each module containing four central and 12 peripheral cells.
- Each module is equipped with a light sensor for input and produces a propulsive force as output, with a single degree of freedom.
- Propulsive force magnitude adjusts based solely on input from the light sensor, without other external information.
- Each module and colony were sufficiently small, resulting in a low Reynolds number, where viscous forces were dominant.

During colony rotation, modules experience light stimulation, resulting in a sine wave pattern. Thus, we assumed that each module can estimate the current rotation period as $P_i(t)$ [s].

2.3. Statement of the Problem

This study aimed to construct a modular control method that allowed adaptive and purposive self-organization of behavior within the constraints of autonomous and decentralized modular control. The objective behavior was phototaxis, i.e., swimming toward the direction of the light. Because the swimming direction must be correctly aligned, we assessed the phototaxis performance based on the time taken for the colony to turn toward the right direction when it was oriented at 90° to the direction of light.

Success was defined as correct orientation within the simulation time, and the success ratio of phototaxis was also assessed.

To analyze the phototactic behavior, we used phase representation to interpret the relationship between the model parameters and its phototaxis performance. We then proposed an adaptive tuning method for the control parameters and optimized the response of the module to achieve fault-tolerant swimming performance, which was robust against module failures.

To verify the improvement in fault tolerance through the proposed method, we conducted simulations under a scenario in which N_f out of 16 modules failed and ceased to generate propulsion.

3. Fault-Tolerant Module Control

3.1. Dynamical Model of Phototaxis of Gonium pectorale

Here, we constructed a phototactic model of Gonium as a modular system.

Therefore, The propulsion force $\boldsymbol{F}(t) \in \mathbb{R}^3$ and viscous force $\boldsymbol{F}_v(t) \in \mathbb{R}^3$, and the torque $\boldsymbol{L}(t) \in \mathbb{R}^3$ and viscous torque $\boldsymbol{L}_v(t) \in \mathbb{R}^3$ of the colony were balanced, respectively, as in Equations (1) and (2).

$$\boldsymbol{F}(t) + \boldsymbol{F}_v(t) = 0 \tag{1}$$

$$\boldsymbol{L}(t) + \boldsymbol{L}_v(t) = 0 \tag{2}$$

As shown in [20], the velocity and angular velocity of a colony, namely $\boldsymbol{U}(t), \boldsymbol{\Omega}(t) \in \mathbb{R}^3$, respectively, are determined by Equations (3) and (4). η and R represent the viscosity of water and the radius of a colony disk, respectively. The parameters k_1,k_3,l_1, and l_3 are dimensionless coefficients that determine the viscous drag along each axial direction.

$$\boldsymbol{F}_v(t) = -\eta R \begin{bmatrix} k_1 & 0 & 0 \\ 0 & k_1 & 0 \\ 0 & 0 & k_3 \end{bmatrix} \boldsymbol{U}(t) \tag{3}$$

$$\boldsymbol{L}_v(t) = -\eta R^3 \begin{bmatrix} l_1 & 0 & 0 \\ 0 & l_1 & 0 \\ 0 & 0 & l_3 \end{bmatrix} \boldsymbol{\Omega}(t) \tag{4}$$

We defined the rotation of the light sensor as the angle β shown in Figure 3a. We defined the coordinate system $\{\boldsymbol{e_1}, \boldsymbol{e_2}, \boldsymbol{e_3}\}$ attached to the colony as shown in Figure 3b.

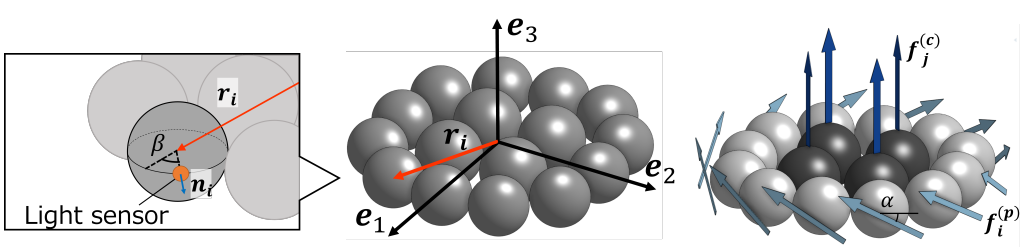

(**a**) (**b**) (**c**)

Figure 3. Structure of the Gonium model with 16 modules, where the spheres represent modules. (**a**) Position of the light sensor. (**b**) Coordinate system $\{\boldsymbol{e_1}, \boldsymbol{e_2}, \boldsymbol{e_3}\}$. $\boldsymbol{r}_i$ is the position vector of module i. (**c**) Propulsive of each module. $\boldsymbol{f}_i^{(\mathrm{p})}$ and $\boldsymbol{f}_i^{(\mathrm{c})}$.

The 12 peripheral modules reduced their own propulsive force in response to the light detected by their own light sensors. Maleprade et al. [20] considered the reaction time until the cell decreased its propulsive force in response to light and the recovery time of the propulsive force. They defined the force-reduction rate using an exponential function. However, Nakajima et al. [24] showed that a model that determined the derivative of the light stimulus as the input and introduced a delay in the response also reproduced the phototactic behavior of Chlamydomonas. Therefore, we simplified the response of the peripheral module to light.

If f_0 and $f_i^{(p)}$ are the magnitudes of the force produced by a single neutral module and $f_i^{(p)}$ of the peripheral module propulsion reduced by light stimuli, respectively, we express the force of the peripheral modules by Equation (5). $I_i(t)$ denotes the input light. We considered a delay time τ_i[s] in response to the light stimuli.

$$f_i^{(p)}(t) = f_0(1 - I_i(t - \tau_i)) \tag{5}$$

The thrust reduction in the four central cells was neglected because of its minimal effect on the change in direction.

In this model, each peripheral module used the derivative of the external light stimuli as its input. Equation (6) represents $I_i(t)$, where I_0 is a constant that donates the sensitivity to the light; β is the orientation shift angle of the light sensors; $\boldsymbol{s} \in \mathbb{R}^3$ is a vector in the direction of light; and $\boldsymbol{n}_i \in \mathbb{R}^3$ is the unit vector in the direction of the light sensor i facing shown in Figure 3a. The 12 peripheral modules are arranged in concentric circles, and $\boldsymbol{n}_i$ is given by Equation (7).

$$I_i(t) = I_0 \frac{d}{dt}\left(\boldsymbol{s}^\top \boldsymbol{n}_i\right) \tag{6}$$

$$\boldsymbol{n}_i = \cos\left(\frac{\pi}{6}i + \beta\right)\boldsymbol{e}_1 + \sin\left(\frac{\pi}{6}i + \beta\right)\boldsymbol{e}_2 \tag{7}$$

The 12 peripheral modules produce force $\boldsymbol{f}_i^{(p)} \in \mathbb{R}^3 (i = 1, \cdots, 12)$ forming an angle α with the colony disk, while the four central modules produce force $\boldsymbol{f}_j^{(c)} \in \mathbb{R}^3 (j = 1, \cdots, 4)$ perpendicular to the colony disk. Figure 3c shows a geometric view of these forces, where the dark and light gray spheres represent the central and peripheral modules, respectively. The 12 arrows of $\boldsymbol{f}_i^{(\mathrm{p})}$ surrounding the colony represent the force of the peripheral modules forming angles α with the disk. The four arrows of $\boldsymbol{f}_i^{(\mathrm{c})}$ above represent the forces acting on the central modules. For simplicity, we neglected the reduction in the propulsive force of the central modules, which had little effect on the orientation.

Using the basis vectors of the colony, $\boldsymbol{f}_i^{(p)}$ and $\boldsymbol{f}_j^{(c)}$ can be expressed as follows:

$$\begin{aligned}\boldsymbol{f}_i^{(p)}(t) = &-f_i^{(p)}(t)\cos(\alpha)\sin\left(\frac{\pi}{6}i\right)\boldsymbol{e}_1 \\ &+ f_i^{(p)}(t)\cos(\alpha)\cos\left(\frac{\pi}{6}i\right)\boldsymbol{e}_2 \\ &+ f_i^{(p)}(t)\sin(\alpha)\boldsymbol{e}_3 \quad (i = 1, \cdots 12)\end{aligned} \tag{8}$$

$$\boldsymbol{f}_j^{(c)}(t) = f_0\boldsymbol{e}_3 \quad (j = 1, \cdots 4) \tag{9}$$

Let $\boldsymbol{r}_i \in \mathbb{R}^3$ be the position vector of the module i, where the center of the colony disk is regarded as the origin, as shown in Figure 3b. For simplicity, we neglect the size of the modules and let $|\boldsymbol{r}_i| = R/2$. The propulsion force $\boldsymbol{F}(t)$ and torque $\boldsymbol{L}(t)$ of the entire colony are expressed as follows:

$$\boldsymbol{F}(t) = \sum_{j=1}^{4} \boldsymbol{f}_j^{(c)}(t) + \sum_{i=1}^{12} \boldsymbol{f}_i^{(p)}(t) \tag{10}$$

$$\boldsymbol{L}(t) = \sum_{i=1}^{12} (\boldsymbol{r}_i \times \boldsymbol{f}_i^{(p)}(t)) \tag{11}$$

Solving the above Equations (1)–(11) yields $\boldsymbol{U}(t)$ and $\boldsymbol{\Omega}(t)$.

3.2. Phase-Based Tuning of τ_i

As mentioned above, the effect of delay time on phototaxis has been previously discussed [24,25]. The timescale of the photoresponse of Volvocine algal cells corresponds to the angular velocity of rotation [26]. Therefore, it is reasonable to treat the delay time of the photoresponse τ_i as a controllable parameter.

We interpreted the relationship between the delay time $\tau_i(t)$ and phototaxis in terms of the phase and proposed a tuning method for $\tau_i(t)$ aimed at optimizing phototactic responsiveness.

For phototaxis, the propulsive force must be reduced when the module faces light and increased again when it faces the opposite direction. If the light sensors of the modules are located straight outward and the modules receive the light stimulus itself as the input, they do not need to shift the phase of the increase/decrease in the propulsive force or the phase of the input. However, the input $I_i(t)$, which is the derivative of the light stimulus, produces a sine wave shifted in phase by $\pi/2$. Furthermore, considering that the position of the light sensor shifts by β, the modules must shift the phase of the increase/decrease of the propulsive force and that of the input $I_i(t)$.

The required phase shift for positive phototaxis $\Delta\theta_\mathrm{p}$ is

$$\Delta\theta_\mathrm{p} = \pi/2 - \beta \tag{12}$$

To achieve negative phototaxis, the phase must be inverted from that of positive phototaxis. Hence, the required phase shift for negative phototaxis $\Delta\theta_\mathrm{n}$ is given by

$$\Delta\theta_\mathrm{n} = 3\pi/2 - \beta \tag{13}$$

By tuning $\tau_i(t)$, as shown in (14), $\tau_j^*(t)$ achieves optimal phototaxis; here, $\Delta\theta = \Delta\theta_\mathrm{p}$ for positive phototaxis, and $\Delta\theta = \Delta\theta_\mathrm{n}$ for negative phototaxis.

$$\tau_i^*(t) = -\frac{\Delta\theta_\mathrm{p,n}}{2\pi} P_i(t) \tag{14}$$

Figure 4 depicts the schematic of the proposed control. Each module separately tunes $\tau_i^*(t)$ from the estimated rotation period $P_i(t)$.

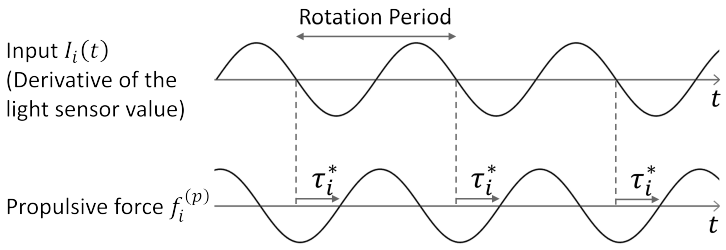

Figure 4. Schematic of phase-based control.

The rotation period fluctuated because some cells were missing or non-functional. Hence, without appropriate phase shifting by controlling the time delay according to $P_i(t)$, the phototaxis performance may be reduced, or phototaxis may not occur. Therefore, $\tau_i(t)$ must be tuned as $\tau_i(t) = \tau_i^*(t)$ for fault tolerance.

4. Verification of the Phase-Based Control

4.1. Verification of the Model

First, we verified that the proposed model adequately reproduced positive and negative phototaxis using the phase-based tuning of τ_i.

We used MATLAB R2023a with a time step of 0.02 s. The light was oriented along the negative z-axis $\boldsymbol{s} = (0\ 0\ -1)^\top$. We set the parameters as listed in Table 1 by referring to [20].

Table 1. Parameter settings referring to [20].

Parameter	Value
η [mPa·s]	1
R [μm]	40
f_0 [pN]	7.0
α [rad]	$\pi/6$
β [rad]	$\pi/4$
I_0	0.25
k_1	10
k_3	13
l_1	6
l_3	8

First, we applied constant values for τ_i, namely 0.28 and 1.38, which were derived as τ_i^* for positive and negative phototaxis, respectively. The simulation time was limited to 30 s. The initial position and initial attitude $\boldsymbol{e}_3$ of a colony were set as $(0,0,0)^\top$ and $(1,0,0)^\top$, respectively. Owing to the symmetrical shape of the colony, the results were unaffected by differences in the initial rotation phase.

Figure 5a,b show the trajectories of the colonies. For $\tau_i = 0.28$, a colony swam toward to the light, as well as in the opposite direction for $\tau_i = 1.38$. The model colony exhibited both positive and negative phototaxis depending on τ_i.

We examined the correspondence between τ_i and swimming orientation. As shown in (15), we define ψ as the angle between the light vector s and attitude of a colony $\boldsymbol{e}_3$. $\psi > \pi/2$ indicates positive phototaxis, whereas $\psi < \pi/2$ indicates negative phototaxis. In the initial state, $\psi = \pi/2$.

$$\psi = \cos^{-1}(\boldsymbol{s}^\top \boldsymbol{e}_3) \tag{15}$$

Next, we conducted simulations using different τ values ranging from 0 to 2 in increments of 0.01. The simulation time was 200 s.

Figure 6a shows ψ corresponding to various τ_i. As expected, the swimming direction (represented by ψ) depends on τ_i. Thus, the colony controls the swimming direction by changing τ_i.

We also measured the time taken to orient toward an appropriate swimming direction. We set thresholds of $9/10\pi$ and $\pi/10$, respectively, for positive and negative phototaxis. Proper phototaxis was assumed to be achieved when ψ became larger than $9/10\pi$ or smaller than $\pi/10$.

Figure 6b shows the time required for the orientation. The results demonstrate that τ_i affects both swimming direction and orientation. From these figures, it can be understood that τ_i =0.28 and 1.38 are reasonable values for positive and negative phototaxis, respectively.

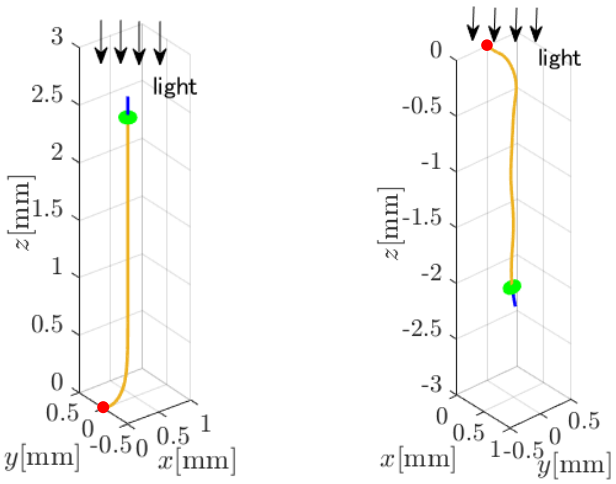

(**a**) (**b**)

Figure 5. Trajectories of phototaxis beginning from the red points. The green disks represent the final state of the colonies, the yellow curves represent the trajectories, the blue lines represent the vector e_3, and the black arrows represent the direction of the light. (**a**) $\tau_i = 0.28$. (**b**) $\tau_i = 1.38$.

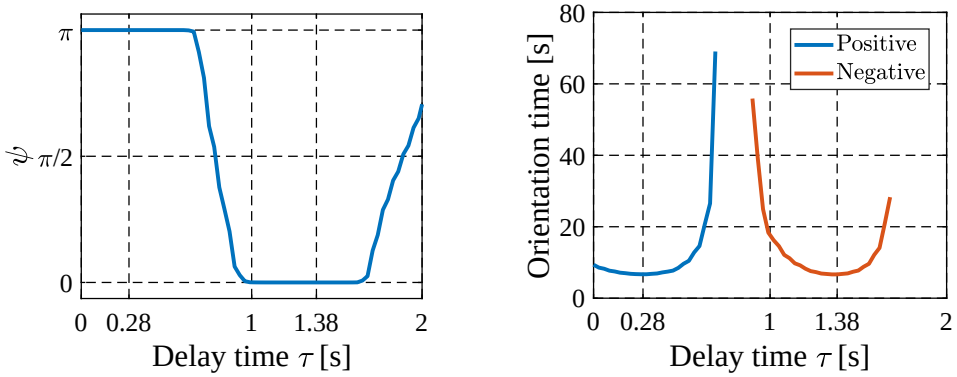

(**a**) (**b**)

Figure 6. Result of phototaxis corresponding to different constant delay times τ_i. (**a**) Angle ψ at steady state. ψ at steady state corresponding to constant τ_i. (**b**) Positive and negative orientation times. Orientation time corresponding to constant τ_i.

4.2. Verification of Fault Tolerance

In this section, we numerically verify that the proposed method improves the fault tolerance in positive and negative phototaxis.

We assumed that out of 16 modules of a colony, N_f modules at random locations failed and lost the propulsion force. We tested N_f = 0 to 8.

We defined a "successful" phototaxis if ψ of a colony was greater than $9/10\pi$ (positive phototaxis) or lesser than $\pi/10$ (negative) within 200 s. We compared fixed $\tau_i(t)$ and $\tau_i^*(t)$ tuned by $\Delta\theta_p$ or $\Delta\theta_n$.

We performed 300 simulations for each condition by randomizing the failed modules using the same parameters as those listed in Table 1.

We performed simulations on the model constructed in the previous section. During this process, we made comparisons under the following three conditions:

- $\tau_i(t) = \tau_i^*(t)$. Each module adaptively tunes its $\tau_i(t)$ according to $P_i(t)$.
- $\tau_i(t)$ is set to a constant derived using Equation (14) under fault-free conditions. $\tau_i(t) = 0.28$ in positive phototaxis, and $\tau_i(t) = 1.38$ in negative phototaxis.
- $\tau_i(t) = 0$. No delay time is considered at all.

Figure 7 shows the success ratio of phototaxis. In the case of positive phototaxis, both fixed τ_i (=0, 0.28) and tuned τ_i^* indicate perfect achievements. In contrast, significant differences are observed in negative phototaxis. Although the tuned τ_i^* remained perfect, the success ratio for fixed τ_i (=1.38) deteriorated when $N_\mathrm{f} > 5$. $\tau_i = 0$ exhibited no negative phototaxis.

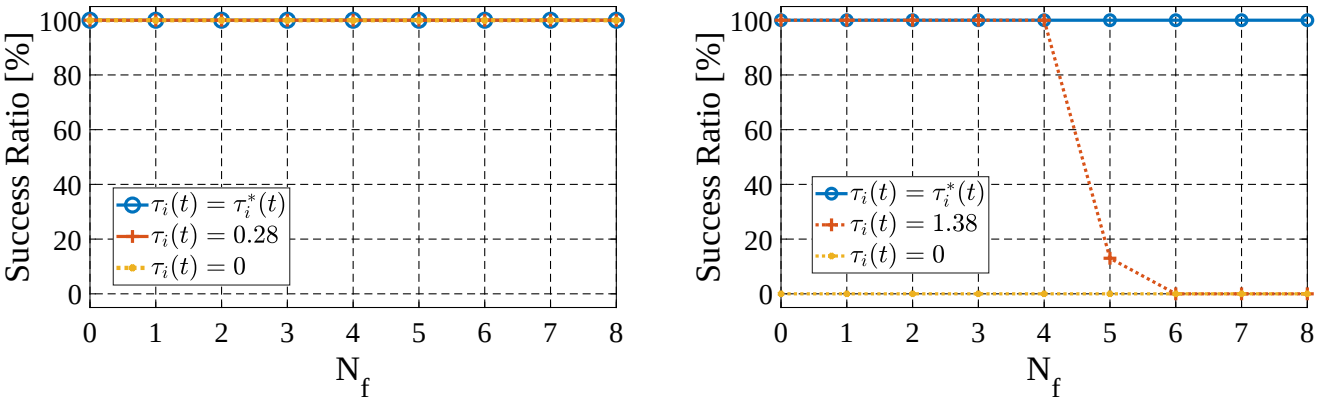

(**a**) (**b**)

Figure 7. Success ratio with failed modules. (**a**) Positive phototaxis, $\tau_i(t) = 0, 0.28$ and $\tau_i(t) = \tau_i^*(t)$. (**b**) Negative phototaxis, $\tau_i(t) = 0, 1.38$ and $\tau_i(t) = \tau_i^*(t)$.

Figure 8 shows the orientation times for positive and negative phototaxis. For positive phototaxis, $N_\mathrm{f} \geq 5$ cases demonstrated significant differences with a significance level of $p < 0.05$ in the Mann–Whitney U test between $\tau_i(t) = \tau_i^*(t)$ and $\tau_i(t) = 0.28$. All N_f cases demonstrated significant differences between $\tau_i(t) = \tau_i^*(t)$ and $\tau_i(t) = 0$. For negative phototaxis, $N_\mathrm{f} \geq 2$ cases exhibited significant differences between $\tau_i(t) = \tau_i^*(t)$ and $\tau_i(t) = 1.38$.

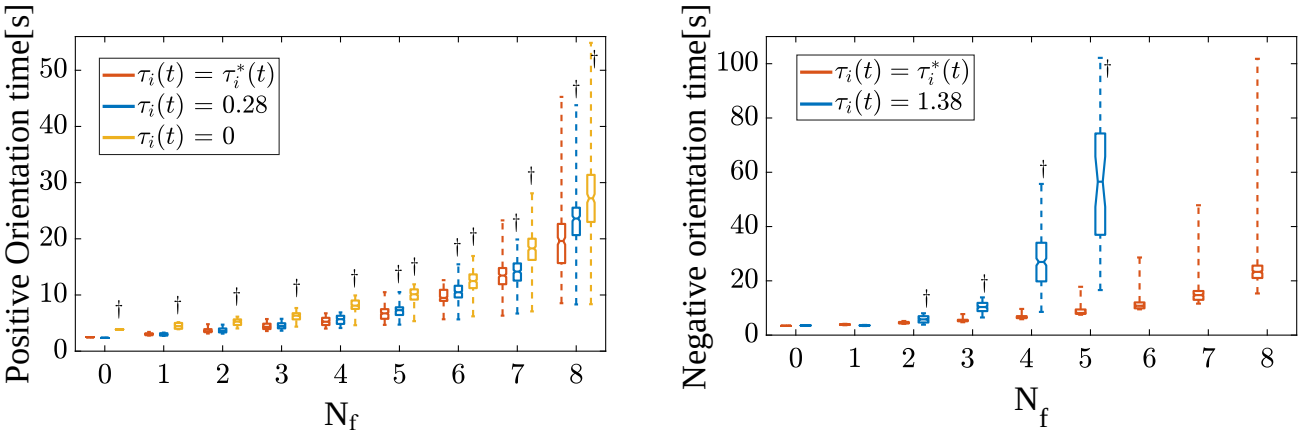

(**a**) (**b**)

Figure 8. Orientation time with failed modules. $^\dagger p < 0.05$. (**a**) Positive phototaxis, $\tau_i(t) = 0, 0.28$ and $\tau_i(t) = \tau_i^*(t)$. (**b**) Negative phototaxis, $\tau_i(t) = 1.38$ and $\tau_i(t) = \tau_i^*(t)$.

5. Discussion

5.1. Fault Tolerance and Sensitivity Analysis

The results in the previous section demonstrate that the proposed method for tuning τ_i improved the fault tolerance of phototaxis exhibited by a colony comprising autonomous distributed modules.

For both the success ratio and orientation time, the difference owing to tuning was more pronounced for negative phototaxis than for positive phototaxis. We hypothesize that

$\Delta\theta_n > \Delta\theta_p$ required a larger phase shift for negative phototaxis, making it more susceptible to variations in the angular velocity of rotation of the colony.

Finally, to verify the generality of this system and control method with respect to parameter values, we conducted simulations with the viscosity coefficients k_1, k_3, l_1, and l_3 all doubled and all increased ten-fold.

The parameter settings follows Table 1 except for k_1, k_3, l_1, and l_3. All the colonies tune $\tau_i(t)$ as $\tau_i^*(t)$. We conducted simulations of positive and negative phototaxis under two conditions shown in Table 2. We set the simulation time to 160 s for condition 1 and 80,000 seconds for condition 2.

Table 2. Viscosity coefficient settings.

Parameter	Condition 1	Condition 2
k_1	20	100
k_3	26	130
l_1	12	60
l_3	16	80

Figure 9a–d show the trajectories of the colonies. Although the temporal and spatial scales differ, both conditions achieved positive and negative phototaxis, and the appearance of the resulting trajectories is almost the same. Therefore, the qualitative properties remain unchanged, confirming that the system is general with respect to the scale of parameters k_1, k_3, l_1, and l_3.

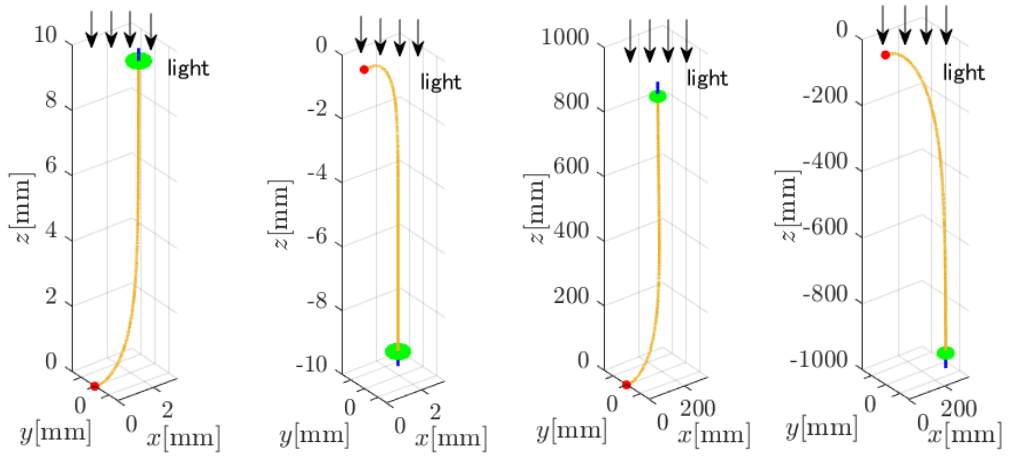

Figure 9. Trajectories of phototaxis with viscosity coefficients doubled (**a**,**b**) and increased ten-fold (**c**,**d**). The colonies start from the red points. The green disks represent the final state of the colonies, the yellow curves represent the trajectories, the blue lines represent the vector e_3, and the black arrows represent the direction of the light. (**a**) Positive phototaxis with condition 1. (**b**) Negative phototaxis with condition 1. (**c**) Positive phototaxis with condition 2. (**d**) Negative phototaxis with condition 2.

5.2. Potential Limitations and Future Work

The verification of the effectiveness of the phase-based control method proposed in this study has been limited to simulations. Additionally, this control method is deeply tied to the module composition and configuration of the modular robot system being controlled and cannot be generally applied to other modular robot systems. The improvement in fault tolerance achieved by this method is limited to self-rotating underwater modular systems,

and it cannot be claimed that we have constructed a general control design framework that enhances fault tolerance for all modular robots.

The previous section's sensitivity analysis has suggested that the qualitative properties of the model and control method remain unchanged even when the scale of the modules and the colony size significantly vary. For further verification of the control method's effectiveness, Further validation will require conducting experiments with actual robots in the future.

The underwater modular system proposed in this study is potentially applicable in environments where human access is difficult, remote operations are restricted, and there is a high possibility of robot component failure during operations. Specifically, this system has potential applications as a radiation source detection system within nuclear power plants.

6. Conclusions

We aimed to construct a robust modular control method for modular robots, which produced autonomous, decentralized, and purposive behavior in a colony. To develop a modular control method for fault-tolerant phototaxis, we constructed a phototaxis model for Gonium and proposed a fault-tolerant module control method for positive and negative phototaxis. The phase-based parameter-tuning method provided a simple interpretation of the relationship between the response time delay and phototaxis. In the proposed method, each module controlled its own response delay using the overall state quantities, angular velocity, and phase of colony rotation.

Simulations confirmed the adequacy of the constructed model and the phase-based control. Simulations under scenarios where random modules failed were also conducted to verify the fault tolerance. In both positive and negative phototaxis, appropriate control over the delay times slowly increased the orientation time when the number of failed modules increased, compared to the case where the delay time was fixed.

The success ratio improved with negative phototaxis. These results confirmed that the proposed autonomous modular control method allowed the colony to maintain its phototactic response even with some failed modules.

However, the transition from simulation-based validation to real-world applications remains crucial. Future research should aim to implement and test these theoretical models in a physical robotic system to confirm whether the control principles proposed in this study are useful for robot phototaxis and fault tolerance, therefore enabling us to realize robust, efficient, and adaptable modular robotic systems.

Author Contributions: Conceptualization, K.N.; methodology, K.N.; software, K.N.; validation, K.N.; writing–original draft preparation, K.N.; writing–review and editing, K.N. and D.K.; visualization, K.N.; supervision, Y.O., H.E. and D.K. All authors have read and agreed to the published version of the manuscript.

Funding: This work was partially supported by the SSUP program of the Sony Semiconductor Solutions Corporation and JSPS KAKENHI under Grant No. JP22H01440 (JP23K22711).

Data Availability Statement: Data are contained within the article.

Acknowledgments: The authors would like to thank Kenichi Wakabayashi for the constructive discussion on the biological observation and models of Gonium algae.

Conflicts of Interest: The authors declare no conflict of interest. The funders had no role in the design of the study; in the collection, analyses, or interpretation of data; in the writing of the manuscript, or in the decision to publish the results.

References

1. Liu, J.; Zhang, X.; Hao, G. Survey on Research and Development of Reconfigurable Modular Robots. *Adv. Mech. Eng.* **2016**, *8*, 1687814016659597. [CrossRef]
2. Saab, W.; Racioppo, P.; Ben-Tzvi, P. A Review of Coupling Mechanism Designs for Modular Reconfigurable Robots. *Robotica* **2019**, *37*, 378–403. [CrossRef]

3. Yim, M.; Shen, W.M.; Salemi, B.; Rus, D.; Moll, M.; Lipson, H.; Klavins, E.; Chirikjian, G.S. Modular Self-Reconfigurable Robot Systems. *IEEE Robot. Autom. Mag.* **2007**, *14*, 43–52. [CrossRef]
4. Feczko, J.; Manka, M.; Krol, P.; Giergiel, M.; Uhl, T.; Pietrzyk, A. Review of the Modular Self Reconfigurable Robotic Systems. In Proceedings of the 2015 10th International Workshop on Robot Motion and Control (RoMoCo), Poznan, Poland, 6–8 July 2015; pp. 182–187. [CrossRef]
5. Murata, S.; Yoshida, E.; Kamimura, A.; Kurokawa, H.; Tomita, K.; Kokaji, S. M-TRAN: Self-Reconfigurable Modular Robotic System. *IEEE/ASME Trans. Mechatron.* **2002**, *7*, 431–441. [CrossRef]
6. Kurokawa, H.; Kamimura, A.; Yoshida, E.; Tomita, K.; Kokaji, S.; Murata, S. M-TRAN II: Metamorphosis from a Four-Legged Walker to a Caterpillar. In Proceedings of the 2003 IEEE/RSJ International Conference on Intelligent Robots and Systems (IROS 2003) (Cat. No. 03CH37453), Las Vegas, NV, USA, 27–31 October 2003; Volume 3, pp. 2454–2459. [CrossRef]
7. Kurokawa, H.; Tomita, K.; Kamimura, A.; Kokaji, S.; Hasuo, T.; Murata, S. Distributed Self-Reconfiguration of M-TRAN III Modular Robotic System. *Int. J. Robot. Res.* **2008**, *27*, 373–386. [CrossRef]
8. Swissler, P.; Rubenstein, M. FireAntV3: A Modular Self-Reconfigurable Robot Toward Free-Form Self-Assembly Using Attach-Anywhere Continuous Docks. *IEEE Robot. Autom. Lett.* **2023**, *8*, 4911–4918. [CrossRef]
9. Alattas, R.J.; Patel, S.; Sobh, T.M. Evolutionary Modular Robotics: Survey and Analysis. *J. Intell. Robot. Syst.* **2019**, *95*, 815–828. [CrossRef]
10. Nainer, C.; Giusti, A. Automatically Deployable Robust Control of Modular Reconfigurable Robot Manipulators. *IEEE Robot. Autom. Lett.* **2022**, *7*, 5286–5293. [CrossRef]
11. Whitman, J.; Travers, M.; Choset, H. Learning Modular Robot Control Policies. *IEEE Trans. Robot.* **2023**, *39*, 4095–4113. [CrossRef]
12. Park, J.H.; Lee, K.H. Computational Design of Modular Robots Based on Genetic Algorithm and Reinforcement Learning. *Symmetry* **2021**, *13*, 471. [CrossRef]
13. Doyle, M.J.; Marques, J.V.A.; Vandermeulen, I.; Parrott, C.; Gu, Y.; Xu, X.; Kolling, A.; Gros, R. Modular Fluidic Propulsion Robots. *IEEE Trans. Robot.* **2021**, *37*, 532–549. [CrossRef]
14. Zhang, T.; Du, Q.; Yang, G.; Wang, C.; Chen, C.Y.; Zhang, C.; Chen, S.; Fang, Z. Assembly Configuration Representation and Kinematic Modeling for Modular Reconfigurable Robots Based on Graph Theory. *Symmetry* **2022**, *14*, 433. [CrossRef]
15. Rubenstein, M.; Ahler, C.; Nagpal, R. Kilobot: A Low Cost Scalable Robot System for Collective Behaviors. In Proceedings of the 2012 IEEE International Conference on Robotics and Automation, Saint Paul, MN, USA, 14–18 May 2012; pp. 3293–3298. [CrossRef]
16. Rubenstein, M.; Cornejo, A.; Nagpal, R. Programmable Self-Assembly in a Thousand-Robot Swarm. *Science* **2014**, *345*, 795–799. [CrossRef] [PubMed]
17. Li, S.; Batra, R.; Brown, D.; Chang, H.D.; Ranganathan, N.; Hoberman, C.; Rus, D.; Lipson, H. Particle Robotics Based on Statistical Mechanics of Loosely Coupled Components. *Nature* **2019**, *567*, 361–365. [CrossRef] [PubMed]
18. Rüffer, U.; Nultsch, W. High-Speed Cinematographic Analysis of the Movement of Chlamydomonas. *Cell Motil.* **1985**, *5*, 251–263. [CrossRef]
19. Ueki, N.; Matsunaga, S.; Inouye, I.; Hallmann, A. How 5000 Independent Rowers Coordinate Their Strokes in Order to Row into the Sunlight: Phototaxis in the Multicellular Green Alga Volvox. *BMC Biol.* **2010**, *8*, 103. [CrossRef] [PubMed]
20. De Maleprade, H.; Moisy, F.; Ishikawa, T.; Goldstein, R.E. Motility and Phototaxis of *Gonium* Simplest Differentiated Colonial Alga. *Phys. Rev. E* **2020**, *101*, 022416. [CrossRef] [PubMed]
21. Coleman, A.W. A Comparative Analysis of the Volvocaceae (Chlorophyta). *J. Phycol.* **2012**, *48*, 491–513. [CrossRef] [PubMed]
22. Isogai, N.; Kamiya, R.; Yoshimura, K. Dominance between the Two Flagella during Phototactic Turning in Chlamydomonas. *Zool. Sci.* **2000**, *17*, 1261–1266. [CrossRef]
23. Greuel, B.T.; Floyd, G.L. Development of the Flagellar Apparatus and Flagellar Orientation in the Colonial Green Alga *Gonium pectorale* (Volvocales). *J. Phycol.* **1985**, *21*, 358–371. [CrossRef]
24. Nakajima, M.; Iizuka, K.; Takahashi, R.; Ueki, N.; Isu, A.; Yoshimura, K.; Nakagaki, T.; Hisabori, T.; Sato, K.; Wakabayashi, K.I. Basis for the Phototaxis Sign Reversal in the Green Alga *Chlamydomonas reinhardtii* Studied by High-Speed Observation. 2020. Available online: https://www.biorxiv.org/content/10.1101/2020.12.06.414052v2 (accessed on 5 May 2024).
25. Drescher, K.; Goldstein, R.E.; Tuval, I. Fidelity of Adaptive Phototaxis. *Proc. Natl. Acad. Sci. USA* **2010**, *107*, 11171–11176. [CrossRef] [PubMed]
26. Leptos, K.C.; Chioccioli, M.; Furlan, S.; Pesci, A.I.; Goldstein, R.E. Phototaxis of *Chlamydomonas* Arises from a Tuned Adaptive Photoresponse Shared with Multicellular Volvocine Green Algae. *Phys. Rev. E* **2023**, *107*, 014404. [CrossRef] [PubMed]
27. Umen, J.G. Volvox and Volvocine Green Algae. *EvoDevo* **2020**, *11*, 13. [CrossRef] [PubMed]